Porohyperelastic finite element model for the kangaroo humeral head cartilage based on experimental study and the consolidation theory

N. Thibbotuwawa[1], T. Li[1], *Y.T. Gu[1]

[1]School of Chemistry, Physics and Mechanical Engineering
Queensland University of Technology, Brisbane, QLD, 4001, Australia.
*Corresponding author: yuantong.gu@qut.edu.au

Abstract

Solid-extracellular fluid interaction is believed to play an important role in the strain-rate dependent mechanical behaviors of shoulder articular cartilages. It is believed that the kangaroo shoulder joint is anatomically and biomechanically similar to human shoulder joint and it is easy to get in Australia. Therefore, the kangaroo humeral head cartilage was used as the suitable tissue for the study in this paper. Indentation tests from quasi-static (10^{-4}/sec) to moderately high strain-rate (10^{-2}/sec) on kangaroo humeral head cartilage tissues were conduced to investigate the strain-rate dependent behaviors. A finite element (FE) model was then developed, in which cartilage was conceptualized as a porous solid matrix filled with incompressible fluids. In this model, the solid matrix was modeled as an isotropic hyperelastic material and the percolating fluid follows Darcy's law. Using inverse FE procedure, the constitutive parameters related to stiffness, compressibility of the solid matrix and permeability were obtained from the experimental results. The effect of solid-extracellular fluid interaction and drag force (the resistance to fluid movement) on strain-rate dependent behavior was investigated by comparing the influence of constant, strain dependent and strain-rate dependent permeability on FE model prediction. The newly developed porohyperelastic cartilage model with the inclusion of strain-rate dependent permeability was found to be able to predict the strain-rate dependent behaviors of cartilages.

Keywords: Solid-extracellular fluid interaction, Drag force, Strain-rate dependent behavior, Porohyperelasticity, Finite element method

Introduction

In mundane activities such as lifting, throwing etc., shoulder cartilages are subjected to physiologically different strain-rates. It is essential that the shoulder cartilage have the ability to undergo controlled deformation in response to these different external loading conditions. Solid-extracellular fluid interaction is considered to play a significant role in facilitating this behavior of shoulder cartilage tissues by rendering its ability to perform as a mechanically efficient tissue. It is crucial to understand the extent to which solid-extracellular fluid interaction facilitates the strain-rate dependent behavior of shoulder cartilage tissues, in order to identify its implications for initiation of shoulder osteoarthritis and development of artificial shoulder cartilage tissues etc. Therefore, the main objective of the current study is to understand how solid-extracellular fluid interaction facilitates strain-rate dependent behavior of shoulder cartilage tissues.

Evidences from literatures indicated that the mechanical behavior of articular cartilages is strain-rate dependent (Finlay and Repo 1979; Lai et al. 1981; Oloyede and Broom 1992; Oloyede et al. 1992; Radin et al. 1970; Woo et al. 1980). According to experimental findings, with increasing strain-rate, the stiffness quickly increases at the beginning and then obtains an

asymptotic value (Oloyede et al. 1992). The interplay between solid and fluid contributes significantly to this behavior with 70%-80% of the load being supported by the matrix at low strain-rates (Oloyede and Broom 1992), while fluid contributes to a similar percentage at large strain-rates (Li and Herzog 2004; Oloyede and Broom 1992). Researchers have different opinions regarding the mechanisms underlying the strain-rate dependent behavior of cartilage tissues. Back in 1980's, McCutchen (1982) argued that this apparent time-dependent behavior is solely related to the volume loss due to water exudation from the cartilage matrix, rather than the intrinsic viscoelasticity of the matrix. Oloyede et al. (1992) substantiated the argument of McCutchen (1982) by loading the cartilage from quasi-static to impact strain-rates and observed a poroelastic behavior at low strain-rates and elastic behavior at impact strain-rate. Therefore, they claimed that the apparent viscoelastic behavior is due to the drag forces introduced by reduction of permeability with strain and solid-extracellular fluid frictional interactions (Oloyede and Broom 1996). DiSilvestro et al.(2001) proposed that the flow-independent viscoelastic mechanism is the main contributor to the strain-rate dependent behaviors of cartilage. Based on the close confirmation of Biphasic-poroviscoelastic FE model to experimental results, they concluded that the mechanism underlying the strain-rate dependency is dominated by the viscoelasticity of matrix material. Considering the cartilage as a fiber reinforced composite material, Li et al. (2003) claimed that the fluid flow can induce fibril stiffening, which is the main mechanism governing the strain-rate dependent behaviors.

The main argument of Li et al.'s (2003) study is that, the models that do not distinguish between fibrils and proteoglycans are not able to capture the nonlinear transient response of cartilage tissue. They have further argued that the ratio of maximum transient stiffness to equilibrium stiffness has a limitation (<1.5) in models that do not distinguish between fibrils and proteoglycans, hence are not adequate to study the tissue response at high strain-rates. Although biphasic theory (Mow et al. 1980) comprises of those limitations, the porohyperelastic model -based on Biot's (1941) theory which is used in this paper does not have these limitations. Further, hyperelastic material model used in this study to represent solid skeleton is capable of improving the model deviations such as decrease in stiffness observed in fibril reinforced model (Li et al. 2003) at large strains. Compared to the poroviscoelastic model (DiSilvestro et al. 2001), the current model is able to explain the experimental observation without adopting viscoelastic theories.

In this study, we follow the same arguments as of McCutchen (1982) and Oloyede and Broom (1996). Hence we believe that the drag forces and solid-extracellular fluid interaction is the main reason of apparent strain-rate dependent behavior of shoulder cartilage tissues. In order to test this hypothesis, a FE model was developed under the poromechanics framework of Biot (1941) and the modeling results are compared to the experimental results obtained through indentation testing under different strain-rates.

Experimental animal model for shoulder cartilage

Choice of animal model for shoulder cartilage tissue requires the shoulder joint of the animal model to be anatomically and biomechanically similar to that of human joint. Also sufficient tissue thickness is required for the macro scale testing to be carried out. Quadruped animal use forelimbs for weight bearing activities. However, humans do not use forelimbs (shoulder joints) much for weight bearing activities. Therefore, macropods, rat and certain species of mice (kangaroo mice, dipodids, springhare and hopping mice) are the animal models that can be considered to have anatomically and biomechanically similar shoulders to humans. Tissue

thickness of rat and mice are not sufficient for macroscopic testing. In macropod family, tree kangaroo, which is a rare species, is known to have a similar anatomy and biomechanics to that of a human shoulder (Sonnabend and Young 2009). Considering these facts kangaroo was chosen as the suitable animal model for the current study.

Experimental methodology

Tissue harvesting, preparation and thickness measurements

Visually normal, kangaroo cartilage samples of 8mm diameter with 2-3mm of subchondral bone intact were harvested using a specially designed stainless steel puncher. The samples were obtained from central load bearing area of the humeral heads (Fig. 1a). The specimens were harvested from five adult kangaroos (approximately 5 years old) within 24 hours of slaughtered, from an abattoir (Fig. 1b). Until testing, all samples were wrapped around a 0.15M saline wetted towel and stored at -20°C. The sides of cartilage on bone samples were visualized through a microscope (Olympus SZ40, Tokyo, Japan) for magnification purposes and uncalcified cartilage thickness was measured using high precision vernier caliper. Measurements were taken from eight locations of approximately equal gaps around the perimeter and final thickness of cartilage was taken as the mean of measurements.

Indentation testing

Subchondral bone underneath the cartilage sample was properly constrained using stainless steel holder (Fig. 1c), to ensure that the deformation data obtained is only due to the deformation of the cartilage. Prior to testing, all the samples were thawed in 0.15M saline for 1.5 hours. The indentation testing was carried out at 10^{-4} s^{-1}, $5x10^{-4}$ s^{-1}, $5x10^{-3}s^{-1}$ and $10^{-2}s^{-1}$ strain-rates (Fig. 1d). The samples were indented up to 30% engineering strain. A limit of 3MPa was imposed on the amount of stress that samples were subjected to, in order to minimize the damage to the tissues (Morel and Quinn 2004; Quinn et al. 2001). However, none of the cartilage samples attained this limit of stress during the strain-rates tested. The testing was done on Instron testing machine (Model 5944, Instron, Canton, MA) using a plane ended polished indenter of 3mm diameter.. Depending on the thickness of the samples, the speed of the Instron machine was adjusted to obtain the required strain-rate. After each test, prior to the next one, the cartilage was unloaded and allowed to recover for 2 hours in 0.15M saline.

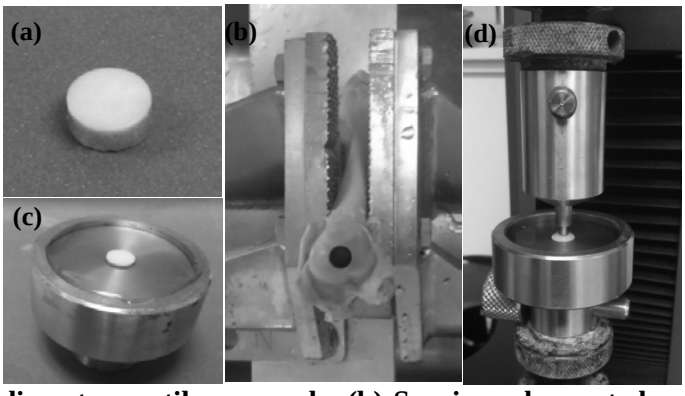

Figure 1 (a) 8mm diameter cartilage sample. (b) Specimen harvested region: Central humeral head. (c) Bone is constrained using a stainless steel holder arrangement. (d) Indentation testing on sample

Pertinent porohyperelastic theory

The governing equations of Biot's (1941) theory for cartilage, considering solid skeleton as a hyperelastic material, can be found in Oloyede and Broom (1994) and Oloyede and Broom (1996) and is summarized below. The fluid flow is taken to follow Darcy's law (equation 1).

$$V_{ij} = -K_{ij}\left(\frac{du}{dx}\right) \tag{1}$$

Herein, V_{ij}, K_{ij} and u are fluid velocity, direction dependent permeability and fluid excess pore pressure, respectively. Based on the equation (1), the continuity equation of fluid flow:

$$\psi\left[\frac{\partial}{\partial x}\left(K_x\left(\frac{\partial u_x}{\partial x}\right)\right)+\frac{\partial}{\partial y}\left(K_y\left(\frac{\partial u_y}{\partial y}\right)\right)+\frac{\partial}{\partial z}\left(K_z\left(\frac{\partial u_z}{\partial z}\right)\right)\right]=\frac{\partial(\sigma_{ij}-u)}{\partial t} \tag{2}$$

ψ, K_i and σ_{ij} are matrix bulk moduli, permeability in ith direction and applied stress, respectively. The constitutive law for solid skeleton is as follows.

$$\sigma_{ij} = \sigma_{sij} + u\delta_{ij} \qquad\qquad \sigma_{sij} = \frac{\partial W}{\partial \lambda_{ij}} \tag{3}$$

σ_{sij}, δ_{ij}, λ_{ij} and W are effective solid skeleton stress, Kronecker delta, stretch ratio and isotropic strain energy potential, respectively.

Porohyperelastic FEA model

Cartilage was modeled as a porous media saturated with fluid based on the generalized framework of Biot's (1941) theory. The model was developed in commercial software (ABAQUS 6.12 version). Axisymmetric element (8-node axisymmetric quadrilateral, bilinear displacement and bilinear pore pressure) are adopted to reduce the computational cost based on the characteristics of test sample and loadings. The large deformations and geometric nonlinearity were considered in the calculation. The 'pore pressure (p)' (p=0) boundary condition was enforced on the upper surface of portion where the indenter is not touching the surface and the right side of the cartilage to enable the fluid flow through these boundaries.. The lower boundary of the model was fixed in vertical and lateral direction, to represent the physiological conditions in cartilage-bone interface. As the stiffness of indenter and bone are higher than the cartilage, the indenter and the bone were modeled as rigid bodies for the ease of modeling. The preliminary studies indicated that the material model used for the indenter and bone does not significantly affect the prediction result.

To account for the non-linear large deformation, the solid skeleton was modeled as an isotropic hyperelastic material. The highly nonlinear stress-strain behavior observed during the current study is unable to be represented by lower order hyperelastic material model such as neo-Hookean or Mooney-Rivlin. Higher order hyperelastic material models such as Yeoh model are believed to be more suitable in explaining the nonlinearity of cartilage tissues (Oloyede et al. 2009). However, 2nd order polynomial hyperelastic function gave an accurate description of the material behavior observed during this study, for humeral head cartilage tissues. Due to lesser number of parameters in 2nd order polynomial hyperelastic function, Inverse FE procedure can be implemented to obtain unique set of material parameters. The general functional form of hyperelastic materials is:

$$W = \sum_{i+j=1}^{N} C_{ij}(\bar{I}_1 - 3)^i(\bar{I}_2 - 3)^j + \sum_{i=1}^{N} \frac{1}{D_i}(J-1)^{2i} \quad (4)$$

Here, W , $\bar{I}_1$ and $\bar{I}_2$ are isotropic strain energy potential, first and second deviatoric strain invariants, respectively. The J is the volume change during the deformation. C_{ij} and D_i are material parameters related to stiffness and the volumetric change of the cartilage. Setting N=1, the above equation reduces to Mooney-Rivilin model. If for all C_{ij} with $j \neq 0$ are set to zero, then N=1, N=2 and N=3 would represent neo-Hookean, the 2nd order polynomial hyperelastic function and Yeoh models, respectively.

The strain dependent permeability function used in this study is shown in equation 5 where intrinsic permeability (K_0) is related to permeability (K) as follows.

$$K = K_0\left(\frac{e}{e_0}\right)^m exp\left\{\frac{M}{2}\left[\left(\frac{1+e}{1+e_0}\right)^2 - 1\right]\right\} \quad (5)$$

Here e is the void ratio (ratio of volume of pores to volume of solid), a quantity representing 'dilatation' in ABAQUS. The e_0 is the initial void ratio, which is taken to be 4, based on the assumption that on average 80% of cartilage is filled with pores (Holmes and Mow 1990). The M and m are dimensionless material parameters which were taken to be 4.638 and 0.0848 respectively (Holmes and Mow 1990).

Material parameter identification

Material parameters for the 2nd order polynomial hyperelastic function were obtained using an inverse-FE procedure. Following the approach developed by Simon et al.(1998), stiffness parameters of the 2nd order hyperelastic function, C_{10} and C_{20} were obtained by curve fitting the force-indentation experimental data at highest strain-rate, 10^{-2}/sec, to FE model prediction considering the material as incompressible. On the other hand, considering the material as compressible, parameters related to volumetric change of the 2nd order hyperelastic function D_1 and D_2 were obtained by curve fitting the force-indentation experimental data at lowest strain-rate, 10^{-4}/sec to FE model prediction. Assuming the fluid flow is negligible, the intrinsic permeability of the cartilage was obtained by curve fitting the porohyperelastic FE model prediction to experimental data at lowest strain-rate.

Results and discussion

Biomechanical parameters: Comparison with the literature values

The measured average thickness of kangaroo humeral head cartilage samples was 0.75 ± 0.123mm. The reported thickness value for human shoulder cartilage is 1.44mm (Soslowsky et al. 1992), which is approximately two times higher than that of kangaroo cartilages. Given larger size of humans, these values are reasonable compared to average kangaroos. The 2nd order polynomial hyperelastic function fitted well to the both low and high strain-rate data with R-squared (R^2) vales greater than 0.98. The functional form of the R^2, an error indicator is shown in equation (6).

$$R^2 = 1 - \frac{\sum_i (e_i - f_i)^2}{\sum_i (e_i - \bar{e}_i)^2} \quad (6)$$

Here, e_i is the experimental data and f_i is the FE model prediction. The $\bar{e}_i$ is the mean value of experimental results. The average stiffness parameters, i.e. C_{10} and C_{20}, identified from the inverse finite element analysis were 0.1174 ± 0.0884MPa and 0.1367 ± 0.0767MPa, respectively. The average compressibility parameters, i.e. D_1 and D_2 were 0.0982 ± 0.0588MPa and 0.0636 ± 0.0407MPa. The permeability value identified from the average data of the lowest strain-rate is $7.62\text{x}10^{-8}$mm/sec. The value of permeability obtained through inverse-FE procedure is at the same order with that reported in the literature for the central region of the humeral head cartilage, which is $1.82\pm1.27\text{x}10^{-8}$ mm/sec (Huang et al. 2005). The hyperelastic material parameters for shoulder cartilage tissues have not been reported elsewhere. Nevertheless, since μ (shear modulus) = $2C_{10}$ and assuming Poisson's ratio to be 0.15 (Demarteau et al. 2006; Korhonen et al. 2002), Young's modulus (E) for the average data of this study is obtained to be 0.485MPa. This value is within the range (0.28-0.8MPa) reported for bovine humeral head cartilage (Demarteau et al. 2006; Korhonen et al. 2002). The calculated E for human shoulder cartilages from reported compressive modulus (H_A) (Huang et al. 2005) using equation (7) is 0.142MPa. The Poisson's ratio (υ) was also taken to be 0.15 in this calculation. This value is 3 times smaller than the calculated values in our study. Considering the possible differences in thickness and compositions of cartilages in different species we would consider the value obtained for E in this study is acceptable.

$$H_A = \frac{E(1-\upsilon)}{(1+\upsilon)(1-2\upsilon)} \tag{7}$$

Porohyperelastic FE model: Effect of solid-extracellular fluid interaction and drag force

The comparison of average experimental stress-strain response to the porohyperelastic FE model prediction is shown in Figure 2a and 2b for the cases of constant and strain dependent permeability. In general, both models showed the strain-rate dependent nature, indicating the ability of the poromechanics framework (Biot 1941) to capture the stain-rate dependency. However, compared to the model with constant permeability, the model with strain dependent permeability is able to capture the experimental results at the three lowest strain-rates (10^{-4}/sec, $5\text{x}10^{-4}$/sec and $5\text{x}10^{-3}$/sec) well. This is mostly evident at $5\text{x}10^{-4}$/sec where significant improvement in R^2value is observed (Fig. 2d). Both constant and strain dependent models were not able to adequately capture the stress-strain variation at 10^{-2}/sec strain-rate. However, the model with strain dependent permeability (R^2 =0.8571) was still able to better capture the variation at 10^{-2}/sec in comparison to the model with constant permeability (R^2=0.7815) (Fig. 2d). Therefore, the strain-rate dependent tissue response from 10^{-4}/sec to $5\text{x}10^{-3}$/sec can be attributed to the solid-extracellular fluid interaction and drag forces induce due to shrinkage of pores during tissue deformation, which is represented by strain dependent permeability.

In addition to the strain dependent permeability, we believe that the strain-rate dependent drag forces should be considered when strain-rates reach an order of 10^{-2}. This could be one of the reasons that the strain dependent permeability model cannot adequately predict the tissue response at the highest strain-rate tested, 10^{-2}/sec. One way to take into account the strain-rate dependent drag forces is to consider permeability as a function of strain-rate. According to equation (2) above and has been mentioned by Oloyede and Broom (1996), the fluid exudation from the cartilage will decrease with increasing in strain-rate. This can be attributed to decrease in permeability with the increase of strain-rate. Inverse FE curve fitting to experimental results of current study at 10^{-2}/sec indicated that, a permeability value of $1.62\text{x}10^{-8}$mm/sec would fit to the experimental results well. This permeability value is approximately 4.7 times smaller than the value ($7.62\text{x}10^{-8}$ mm/sec) at the smallest strain-rate. The permeability values obtained using Inverse FE procedure for $5\text{x}10^{-3}$/sec and $5\text{x}10^{-4}$/sec

were almost the same, which are closer to 3.62×10^{-8} mm/sec. This indicates that the effect of strain-rate on permeability at these relatively low strain-rates is negligible. Therefore, for strain-rates larger than 10^{-2}/sec, inclusion of drag forces through the strain-rate dependent permeability is reasonable. Similar phenomena has earlier been postulated by Oloyede and Broom (1992). According to their experimental observations, they have stated, "a comparison

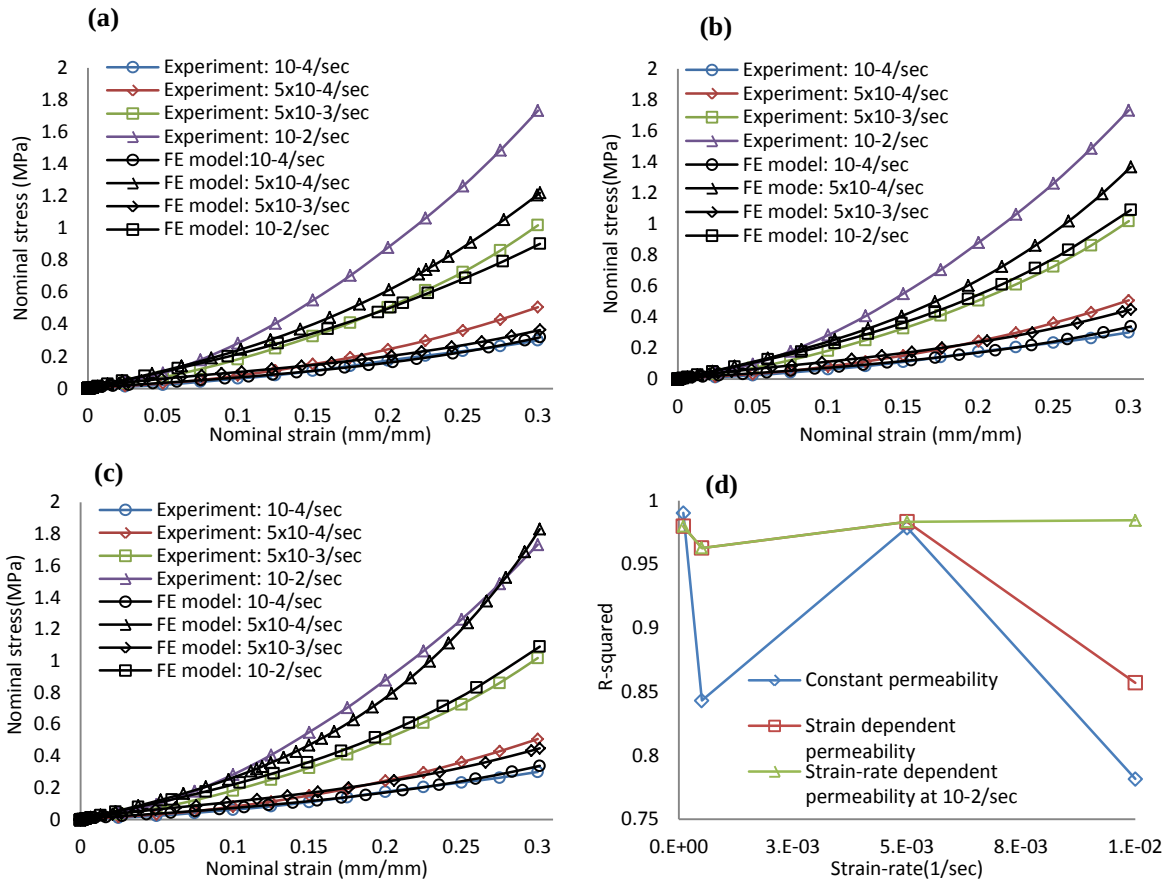

Figure 2. Comparison of FE model prediction to experimental data. (a) Constant permeability (b) Strain dependent permeability (c) With the inclusion of strain-rate dependent permeability at 10^{-2}/sec (d) R-squared values for strain-rates tested

of the effective stress and excess pore pressure curves reveals a distinct dissimilarity in their relationship as the strain-rate is increased from $10^{-3}sec^{-1}$ to $10^{-2}sec^{-1}$". The obtained model results after inclusion of strain-rate dependent permeability is shown in Figure 2c. The experimental results are well predicted by the model (R-squared > 0.96) (Fig. 2d).

In finding further evidence for the underlying mechanism of the above mentioned observations, higher pore pressure value is observed for the case of strain-rate dependent permeability with comparison to strain dependent permeability, at 10^{-2}/sec rate (Fig. 3a and 3b). Moreover, the smaller fluid velocities observed in strain-rate dependent case (Fig. 3c) reflects higher drag forces. Therefore, over and above a certain strain-rates (between 5×10^{-3}/sec - 10^{-2}/sec) will significantly reduce the mobility of the fluid leading to literally lock the fluid inside the tissue. We believe that this locking effect will become more prominent at larger stain-rates, causing the tissues to act as purely elastic solid, as evident by the experimental findings of Oloyede et al. (1992).

In summary, the present study has investigated how solid-extracellular fluid interaction facilitates the strain-rate dependent behavior of shoulder cartilage tissues. The porohyperelastic FE model prediction has been compared with indentation tests on kangaroo

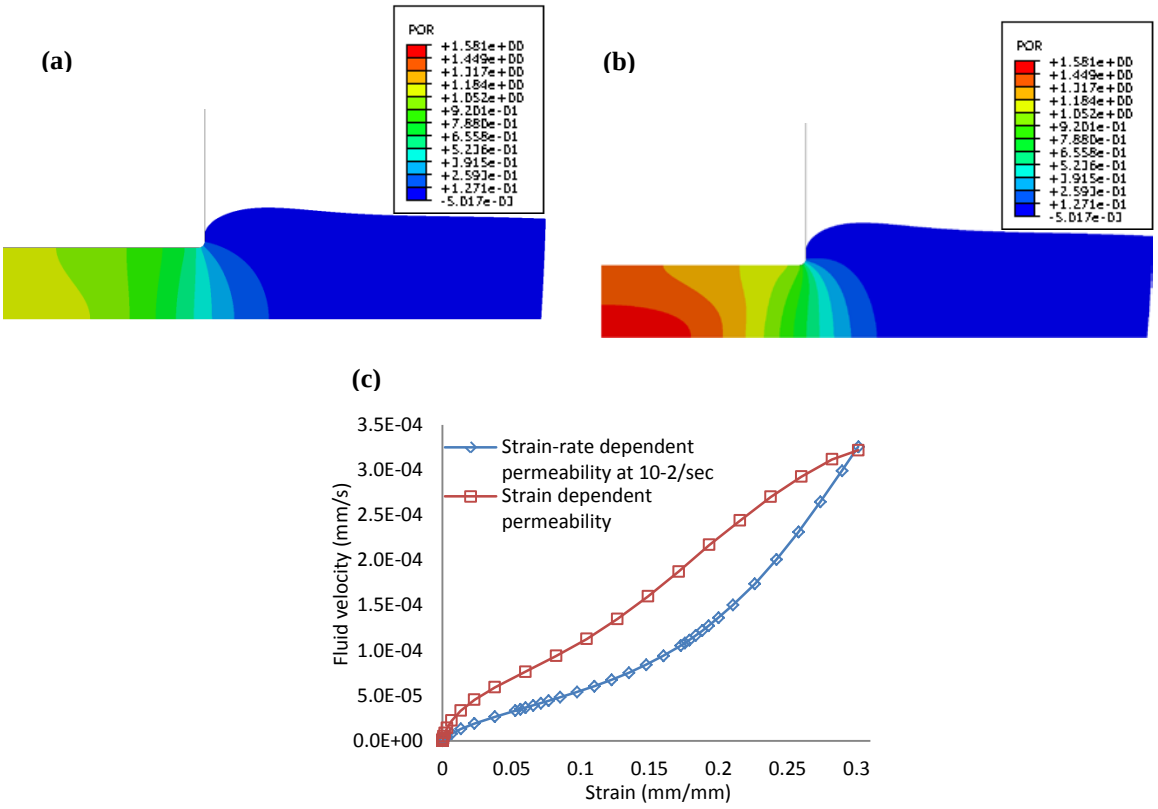

Figure 3. Pore pressure profiles (a) At 10-2/sec: strain-dependent permeabilty. (d) At 10-2/sec: strain-rate dependent (c) fluid velocity at the bottom left of cartilage matrix

humeral head cartilage under quasi-static to high strain-rates. The effect of constant permeability, strain dependent permeability and strain-rate dependent permeability on FE model prediction has been considered with the objective of investigating the effect of solid-extracellular fluid friction forces and drag forces on strain-rate dependent behavior. According to the current investigation when a tissue is deformed under a given strain-rate, shrinking pores will restrict the fluid motion, hence solid-extracellular fluid frictional interaction forces and drag forces will be generated. The magnitude of these forces will depends on the strain, strain-rate, the structure of the pore network and the size of the pores. At higher strain-rates, permeability will reduce significantly due to large drag forces, locking the fluid inside the tissue.

Conclusion

Strain-rate dependent nature of kangaroo humeral head cartilage tissues from 10^{-4}/sec to 10^{-2}/sec is well captured by a newly developed porohyperelastic FE cartilage model with strain-rate dependent permeability. The model with strain dependent permeability was only able to predict the strain-rate dependency from 10^{-4}/sec to $5x10^{-3}$/sec and was better than the model with constant permeability. The drag forces are believed to be dominating the tissues response from an intermediate strain-rate from $5x10^{-3}$/sec to 10^{-2}/sec. This is the main reason why the strain-rate dependent model is superior at higher strain-rates. Therefore, it is necessary to include the strain-rate dependent permeability in order to predict the tissue response at large strain-rates. Therefore, the strain-rate dependent behavior of shoulder

cartilages can be attributed to solid-extracellular fluid interaction and drag forces. In physiological point of view, reduction of permeability at large strain-rates indicates that the fluid will be locked inside the tissue. This is believed to facilitate the ability of the tissues to function as a protective layer for bone ends injurious loads.

Acknowledgement

Authors would like to gratefully acknowledge the financial support provide by ARC Future Fellowship grant (FT100100172) , technical support given by Ms. Melissa Johnston and Dr. Sanjleena Singh in carrying out the experimentations and Mr. Don church at Game meat processing Pvt. Ltd for their frequent support in providing kangaroo shoulder joints for testing.

References

Biot MA. 1941. General theory of three‐dimensional consolidation. Journal of applied physics 12(2):155-164.

Demarteau O, Pillet L, Inaebnit A, Borens O, and Quinn TM. 2006. Biomechanical characterization and in vitro mechanical injury of elderly human femoral head cartilage: comparison to adult bovine humeral head cartilage. Osteoarthritis Cartilage 14(6):589-596.

DiSilvestro MR, Zhu Q, and Suh J-KF. 2001. Biphasic Poroviscoelastic Simulation of the Unconfined Compression of Articular Cartilage: II—Effect of Variable Strain Rates. Journal of Biomechanical Engineering 123(2):198.

Finlay J, and Repo R. 1979. Energy absorbing ability of articular cartilage during impact. Medical and Biological Engineering and Computing 17(3):397-403.

Holmes M, and Mow V. 1990. The nonlinear characteristics of soft gels and hydrated connective tissues in ultrafiltration. J Biomech 23(11):1145-1156.

Huang CY, Stankiewicz A, Ateshian GA, and Mow VC. 2005. Anisotropy, inhomogeneity, and tension-compression nonlinearity of human glenohumeral cartilage in finite deformation. J Biomech 38(4):799-809.

Korhonen R, Laasanen M, Töyräs J, Rieppo J, Hirvonen J, Helminen H, and Jurvelin J. 2002. Comparison of the equilibrium response of articular cartilage in unconfined compression, confined compression and indentation. J Biomech 35(7):903-909.

Lai W, Mow VC, and Roth V. 1981. Effects of nonlinear strain-dependent permeability and rate of compression on the stress behavior of articular cartilage. Journal of biomechanical engineering 103(2):61-66.

Li LP, Buschmann MD, and Shirazi-Adl A. 2003. Strain-rate Dependent Stiffness of Articular Cartilage in Unconfined Compression. Journal of Biomechanical Engineering 125(2):161.

Li LP, and Herzog W. 2004. Strain-rate dependence of cartilage stiffness in unconfined compression: the role of fibril reinforcement versus tissue volume change in fluid pressurization. J Biomech 37(3):375-382.

McCutchen C. 1982. Cartilage is poroelastic, not viscoelastic (including and exact theorem about strain energy and viscous loss, and an order of magnitude relation for equilibration time). J Biomech 15(4):325-327.

Morel V, and Quinn TM. 2004. Cartilage injury by ramp compression near the gel diffusion rate. Journal of orthopaedic research 22(1):145-151.

Mow V, Kuei S, Lai W, and Armstrong C. 1980. Biphasic creep and stress relaxation of articular cartilage in compression: theory and experiments. Journal of biomechanical engineering 102(1):73-84.

Oloyede A, and Broom N. 1992. Stress-sharing between the fluid and solid components of articular cartilage under varying rates of compression. Connective tissue research 30(2):127-141.

Oloyede A, and Broom N. 1996. The biomechanics of cartilage load-carriage. Connective tissue research 34(2):119-143.

Oloyede A, and Broom ND. 1994. The generalized consolidation of articular cartilage: an investigation of its near-physiological response to static load. Connective tissue research 31(1):75-86.

Oloyede A, Crawford RW, Moody HR, Nguyen TC, and Brown CP. 2009. Assessment of common hyperelastic constitutive equations for describing normal and osteoarthritic articular cartilage. Proceedings of the Institution of Mechanical Engineers, Part H: Journal of Engineering in Medicine 223(6):643-652.

Oloyede A, Flachsmann R, and Broom ND. 1992. The dramatic influence of loading velocity on the compressive response of articular cartilage. Connective tissue research 27(4):211-224.

Quinn T, Allen R, Schalet B, Perumbuli P, and Hunziker E. 2001. Matrix and cell injury due to sub‐impact loading of adult bovine articular cartilage explants: effects of strain rate and peak stress. Journal of orthopaedic research 19(2):242-249.

Radin EL, Paul IL, and LowY M. 1970. A comparison of the dynamic force transmitting properties of subchondral bone and articular cartilage. The Journal of Bone & Joint Surgery 52(3):444-456.

Simon B, Kaufmann M, McAfee M, Baldwin A, and Wilson L. 1998. Identification and determination of material properties for porohyperelastic analysis of large arteries. Journal of biomechanical engineering 120(2):188-194.

Sonnabend D, and Young A. 2009. Comparative anatomy of the rotator cuff. Journal of Bone & Joint Surgery, British Volume 91(12):1632-1637.

Soslowsky LJ, Flatow EL, Bigliani LU, and Mow VC. 1992. Articular geometry of the glenohumeral joint. Clinical Orthopaedics and Related Research 285:181-190.

Woo S-Y, Simon B, Kuei S, and Akeson W. 1980. Quasi-linear viscoelastic properties of normal articular cartilage. Journal of biomechanical engineering 102(2):85-90.